Satellite Characterization, Classification, and Operational Assessment Via the Exploitation of Remote Photoacoustic Signatures

Justin Spurbeck[1]
The University of Texas at Austin
Moriba K. Jah, Ph.D.[2]
The University of Texas at Austin
Daniel Kucharski, Ph.D.[3]
Space Environment Research Centre & The University of Texas at Austin
James C. S. Bennett, Ph.D.[4]
EOS Space Systems & Space Environment Research Centre
James G. Webb, Ph.D.[5]
EOS Space Systems

ABSTRACT

Current active satellite maneuver detection techniques have the ability to detect maneuvers as quickly as fifteen minutes post maneuver for large delta-v when using angles only optical tracking. Medium to small magnitude burn detection times range from 6-24 hours or more. Small magnitude burns may be indistinguishable from natural perturbative effects if passive techniques are employed. Utilizing a photoacoustic signature detection scheme would allow for near real time maneuver detection and spacecraft parameter estimation. We define the acquisition of high rate photometry data as photoacoustic sensing because the data can be played back as an acoustic signal. Studying the operational frequency spectra, profile, and aural perception of an active satellite event such as a thruster fire or any on-board component activation will provide unique signature identifiers that support Resident Space Object (RSO) characterization efforts. A thruster fire induces vibrations in a satellite body which then modulate incident rays of light. If the reflected photon flux is sampled at a sufficient rate, the change in light intensity due to the propulsive event can be detected. Sensing vibrational mode changes allows for a direct timestamp of thruster fire events and thus makes possible the near real time estimation of spacecraft delta-v and maneuver type if coupled with active observations immediately post maneuver. This research also investigates the estimation of other impulse related spacecraft parameters such as mass, specific impulse, and mass flow rate using impulse-momentum and work-energy methods.

1. INTRODUCTION

The space environment near Earth has grown crowded since the dawn of the space age in the late 1950s. Technological advances and decreases in manufacturing costs have led to a significant increase in the space object population. Increased launch frequency by government agencies and the private sector coupled with the sheer number of uniquely controlled payloads that can be included per launch demonstrate the need for a robust system to monitor and protect the space environment. A challenge inherit to the crowded orbital environment is how to effectively predict collision risks and use that information to ensure active satellite survival and compliance with the Inter-Agency Space Debris Coordination Committee (IADC) guidelines. The Joint Space Operations Center (JSpOC) provides conjunction data messages via a global array of sensors to operators with assets that have secondary RSOs within their screening volume. The operators will use this information to maneuver their assets into a safer orbit if required. A good operator will send an ephemeris including the planned maneuver to JSpOC such that they can preemptively screen it against any other secondary RSOs. The screening is to ensure the maneuver does not put the satellite into the path of another

1 Graduate Student, Aerospace Engineering and Engineering Mechanics Department, Cockrell School of Engineering, The University of Texas at Austin, Austin, TX 78712.
2 Associate Professor, Aerospace Engineering and Engineering Mechanics Department, Cockrell School of Engineering, The University of Texas at Austin, Austin, TX 78712.
3 Research Fellow, Space Environment Research Centre, SERC, Canberra, Australia. Visiting Researcher, Institute for Computational Engineering and Sciences, The University of Texas at Austin, Austin, TX 78712.
4 Astrodynamics Group Leader, EOS Space Systems Pty Ltd, Queanbeyan, Australia. Research Program Leader, Space Environment Research Center, Canberra, Australia.
5 Instrument Scientist, EOS Space Systems Pty Ltd, Queanbeyan, Australia.

object, effectively defeating the purpose of the collision avoidance maneuver in the first place. There are, however, instances where an operator does not follow this procedure, and thus maneuvers and potential conjunctions are unpredictable. This situation demonstrates the need for a method to quickly detect when an uncooperative RSO has maneuvered and estimate its new trajectory. If there were such a method, it would not only help reduce potential conjunction risks much sooner, it would also provide data that would allow satellite operational capability assessments.

In addition to the need for near real time monitoring of active satellites, there are still gaps in how both active and inactive RSOs are characterized and uniquely identified. Any source of data that would provide unique signature identifiers based on RSO shape, behavior, mass, or other parameter increases our capability to better understand the RSO population. Thus, this research presents a new method to detect satellite maneuvers in near real time and extends the method to support RSO characterization and spacecraft parameter estimation.

2. PHOTOACOUSTIC SENSING & RSO CHARACTERIZATION

An interesting phenomenon becomes observable if photometric data is collected at a rate above 40kHz. The human ear is capable of discerning frequencies from 20Hz to 20kHz. Thus, an acoustic signal can be generated from the photometric data by converting the frequency content in the light curve to audio. To abide by the Nyquist Theorem, sampling at 40kHz plus a safety margin would recover all naturally discernable sound. We define the acoustic playback of high-rate photometric data as its photoacoustic signature. The light to sound conversion is possible because the photons carry an equivalent information content that an acoustic wave cannot because there is no medium for it to propagate through in the vacuum of space [1][2]. This technique has been proven robust in terrestrial based tests that demonstrated the capability to accurately recover a conversation or song on the radio by collecting the light being modulated by a flexible surface nearby the acoustic source such as a plant leaf [3]. The direct analogy to applying photoacoustic sensing remotely is to imagine a satellite's solar panel as the leaf in the prior example and the thruster fire event as the acoustic source from the radio.

An acoustic signal is made up of its fundamental frequencies and harmonics, so why not analyze the photometric frequency content directly and skip the acoustic conversion step? It turns out the human brain is an amazing pattern recognition machine that still outperforms computers in many signal identification applications [4][5]. An example as to how an acoustic interpretation of an inherently non-acoustic signal supported the characterization of a physical event is seen in the analysis of plasma wave data from the Voyager 1 spacecraft. NASA mission scientists converted the vibrations of dense ionized gas detected by the plasma wave instrument into an acoustic signal. When listening to the audio playback, the scientists noticed a rising tone which helped infer a continuously increasing density profile and thus a detection of interstellar plasma [6].

It is plausible that a machine learning or pattern recognition algorithm could be implemented to uniquely identify RSOs and active satellite events based on the pure frequency content in the photometric data. However, an important step in developing those algorithms would be in correlating the aural perception of the photoacoustic data to physical characteristics, like the Voyager 1 example, and using that interpretation to tune the algorithms. The aural perception of the data can also give clues as to what to look for in the frequency domain. This phenomenon is famously depicted by Hollywood in the movie Contact. When Dr. Clark listens closely to the acoustic interpretation of the anomalous signal coming from Vega, he detects a second signal embedded in the harmonics of the original solely by listening to its acoustic playback which clues the team in on what band to amplify and how to display it. While this exact depiction would likely not be realistic for the weak signals the SETI Institute actually scans for, the ability to naturally interpret a data set through sound is still a powerful tool. The notion that a human must acoustically interpret an RSO's photoacoustic signature to gain insight and be a "human in the loop" similar to a sonar operator's role on a submarine is not the end-all goal of this technique. Instead, the photoacoustic analysis should be used as an enhancement, not a replacement, to the traditional pattern recognition and frequency analysis routines that would be applied to the high-rate photometric data to detect events and uniquely characterize RSOs.

Specific methods to accurately characterize photoacoustic signals may be quite similar to how biometric recognition works. The outgoing photon flux from any one RSO is highly dependent on object geometry, attitude, dynamics, and reflectance properties. Organizing the RSO and RSO event signal information into its unique frequency content, transients, pitch, aural perception, dead zones, harmonics, power level, profile, and other categories would provide the modalities needed to implement a biometric recognition system. These biometric modalities fulfill the universality,

distinctiveness, permanence, and collectability requirements for such a system [7][8]. Fusing these modalities with other known or inferred spacecraft parameters would yield the equivalent of an n-factor authentication system regarding how to properly identify an RSO.

3. MANEUVER DETECTION

Current methods for maneuver detection are often passive techniques that use an algorithm to sample historical ephemeris data and apply statistical methods until it can suggest an object's trajectory has deliberately shifted. Depending on the magnitude of the burn, this sort of event detection can take anywhere from around ninety minutes up to several days to resolve. If the burn is small enough, it may be indistinguishable from the natural perturbative effects [9]. Large maneuvers may cause a complete loss of an object's trajectory and can be tedious to reacquire. An active detection technique for a geosynchronous satellite using ground based optical tracking and sequential estimation tools showed that a delta-v of 1.0 m/s could be detected as soon as 15 minutes after a maneuver while a delta-v of 0.01 m/s could take 12-24 hours to discern with confidence [10].

Collecting high rate photometric data on an active satellite has the potential to detect and characterize on-board operational events. The behavior of the reflected sunlight depends on the dynamics of the satellite. An event such as a thruster fire induces vibrations in the satellite body and if the displacement of any reflective surface is large enough, it will modulate the outgoing photon flux. The change in outgoing photons would signal that an event has occurred and thus, if sampled at a sufficient rate, would provide a method to directly timestamp operational events. In theory, the only time constraints to detecting this type of event are the speed of light and data processing workflow.

To demonstrate a maneuver detection, a 2 kHz light curve was simulated for an active satellite with a basic box-wing model in GEO using a simplified Cook-Torrance reflectance model [11]. Other basic spacecraft parameters and assumptions are listed in Table 1. To simulate a thruster fire event, a 60 Hz shear vibrational mode for the satellite bus and a clamped cantilever mode for the solar panel were induced. Simulating the vibration mode was achieved using a simple oscillation model for the satellite bus and solar panel area unit normal vectors at the desired frequencies as depicted in Fig. 1. The simulation emulates a visualization of common satellite modes as presented in [12].

Table 1. Cook-Torrance model parameters used in generating the light curve

Parameter	Value	Units	Material	C_d	C_s
+X / -X Face Area	6.0	m^2	MLI Kapton	0.04	0.59
+Y / -Y Face Area	8.0	m^2	MLI Kapton	0.04	0.59
+Z / -Z Face Area	12.0	m^2	White Paint/Germanium Kapton	0.80 / 0.28	0.04 / 0.18
Solar Panel Area	15.0	m^2	Solar Cells	0.04	0.04

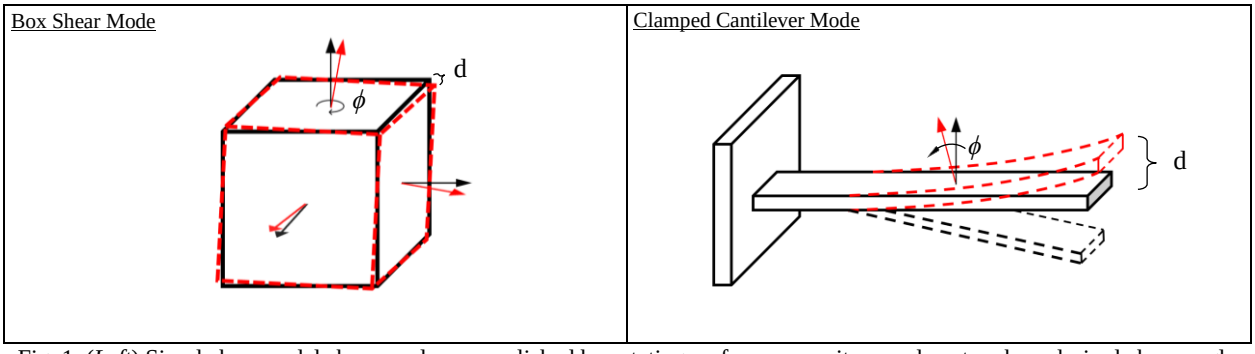

Fig. 1. (*Left*) Simple box model shear mode accomplished by rotating surface area unit normal vectors by a desired shear angle (ϕ). It appears the model is undergoing a simple rotation. However, the three faces not displayed are rotated in the opposite direction, giving the shear effect as expected. (*Right*) Illustration showing a basic beam cantilever vibration mode used for the solar panel. It was assumed there was no flex in the solar panel and thus the axis of rotation about the rigid wing model was at the clamped beam interface.

The displacement magnitudes for these modes would be highly dependent on the material composition, structural geometry, and forcing function imparted by the thruster operation. Instead of building a macro model for a full fidelity

structural vibration simulation, a range of displacement values were run such that a minimum detectable displacement threshold could be defined. A peak reflective surface displacement relative to nominal (d) of at least 3.4 cm or a shear angle (ϕ) of 1.15 degrees shown in Fig. 2 is required to make a detectable change in outgoing photon flux. This estimate assumes a nominal atmospheric turbulence effect on the apparent visual magnitude as a gaussian distribution with zero mean and a very good 0.04 standard deviation. For a more typical standard deviation of 0.10, the maximum displacement required for a detection increases to 13 cm or a 4.30 deg shear angle. Both displacements magnitudes seem quite high for a properly designed satellite. The latter displacement magnitudes for a 60 Hz forcing frequency seem much too large as it would likely be a destructive mode. Thus, the detection probability of a change in reflective surface modulation is highly sensitive to the signal to noise ratio and how the satellite body reacts to a propulsive event. No measurement noise model was implemented as it was assumed the effects of the atmosphere dominated.

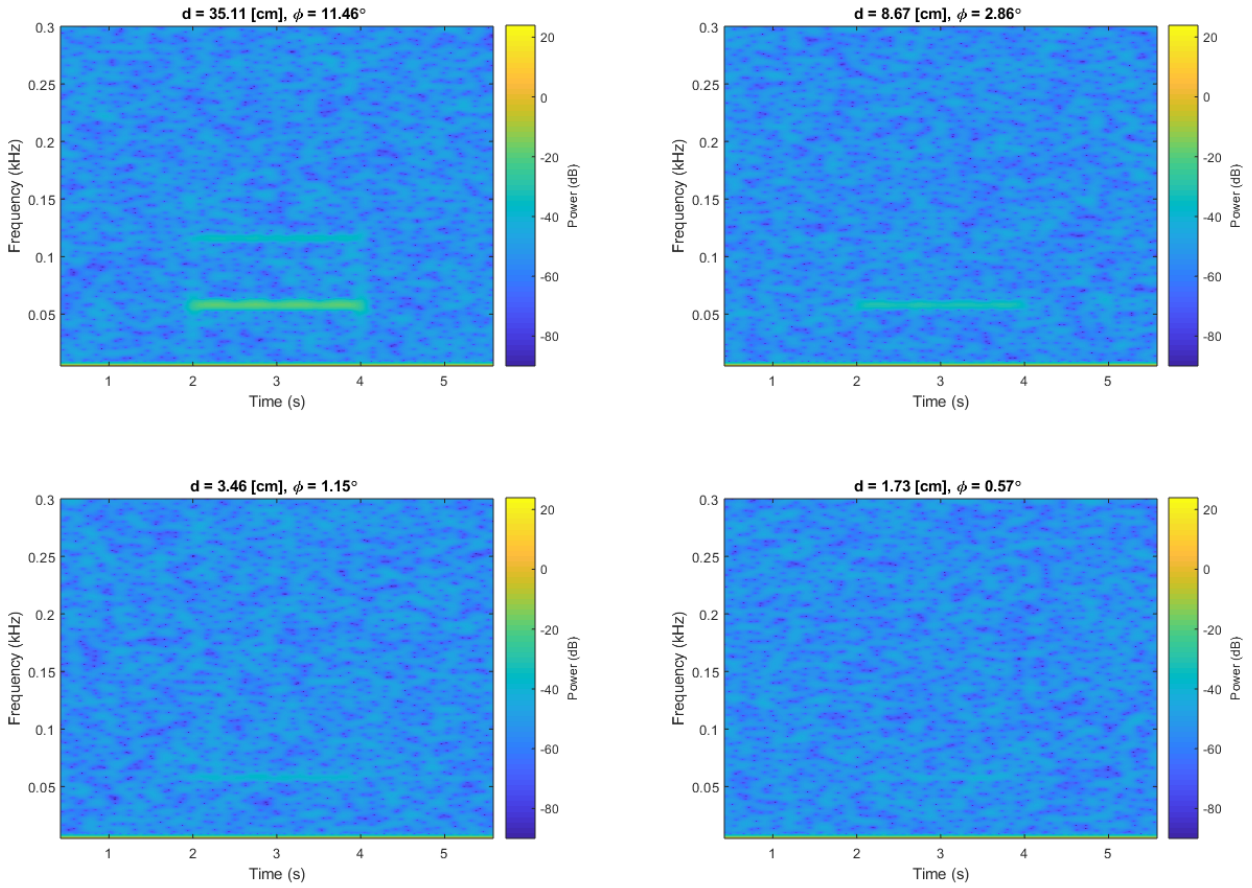

Fig. 2. Fast Fourier Transform (FFT) displayed via spectrogram showing how vibrational mode displacement magnitudes affect event detectability. To cut down on run times, a 2 kHz sampling rate was used. The sub-100 Hz modes are well oversampled at 2 kHz and the acoustic playback was unaffected. Experimentally, these signals may have common measurement system effects like dead zones, harmonics, and other unmodeled noise sources included. The thruster fire event was simulated from 2.0-4.0 seconds. The amplitude of surface modulation decreases from top-down and left-right respectively. (*Top Left*) As expected, the largest surface modulation results in the strongest signal. The amplitude is large enough that a second signal at double the fundamental appears, likely due to another two facets of the box-wing model becoming observable. Displacements this large would be unrealistic but are still included as an extreme case demonstration. (*Top Right*) Decreasing displacement magnitude decreases signal strength. (*Bottom Left*) The minimum detectable displacement criteria defined as a 1.15 deg shear angle. (*Bottom Right*) Likely unable to detect any event with displacements less than 2 cm as the signal would be lost in the noise.

A satellite's mission and instrumentation sensitivity requirements typically define the operational vibration damping requirements. Some operators may not care what the vibrational modes look like during a thruster event, but most active operational modes seem to be greater than 50 Hz for large Earth-imaging or communications satellites. The simulation results show that it is plausible that a thruster fire can be detected via the vibrational modes induced, but it may be difficult and limited to only the lowest frequency modes with large relative displacement on certain parts of the satellite body or solar array. It is also plausible that a maneuver may be detected from observing the thrust plume

and exhaust emissions directly. A final stage booster activation for the AFRL ANGELS satellite mission launch was easily detected with a common DSLR [13]. It's conceivable that the increase in light intensity due to a standard orbital station keeping maneuver would also be detectable with an optical telescope and advanced adaptive optics equipment. The frequency signature and aural perception would likely change for a plume detection. The acoustic playback for the simulations in Fig. 2 yielded simple tonal "humming" sounds for each detection but a plume would likely sound more like a chaotic "fire" type event with more variations in the signature profile.

4. MANEUVER ESTIMATION

For propulsive events, the ability to directly timestamp the impulse allows for estimation of delta-v magnitude, direction, and maneuver type once the state of the RSO is resolved to a desired level of uncertainty post maneuver. We define "near real time" estimation as the time duration between maneuver end and post maneuver state resolution. To study how measurement frequency affects state convergence times post maneuver, an Extended Kalman Filter (EKF) was run with simulated ground-based range and range-rate measurements from three near-equatorial stations for an RSO in a 791 km circular orbit. The simulation included the effects of light time, the same dynamic model discussed below, and used a 5-meter standard deviation for range and 1 mm/s for range rate measurement noise values. For an initial state guess, a 1.0 km offset from the true state was derived and a 4.0 km a priori uncertainty was used for each position component of the covariance matrix. The EKF required 11 observations at 60 second intervals over a span of 27 minutes to achieve a 10-meter 3σ state uncertainty post maneuver as indicated in Fig. 3. The 27-minute span included a 17-minute measurement gap before the satellite was viewable by the next station. Using a 10 second measurement frequency did not improve convergence time.

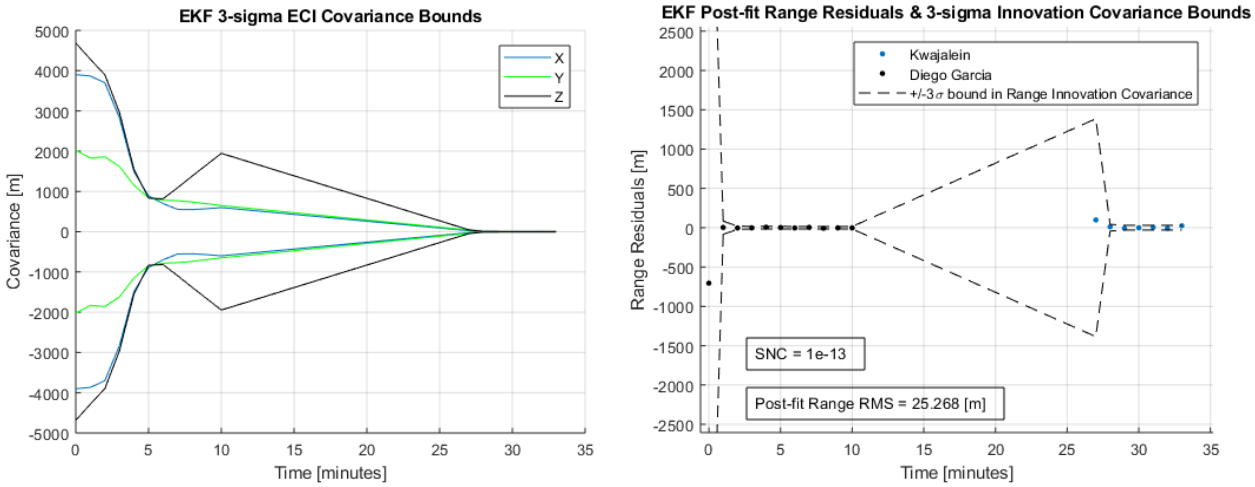

Fig. 3. (*Left*) The ECI covariance behavior assuming a 60 second measurement interval and 17-minute observation gap from 10 to 27 minutes. The observation gap exists because a realistic station location scheme was implemented using Diego Garcia and Kwajalein Atoll sites. The EKF converges to a steady state 10-meter 3σ uncertainty near 27 minutes post maneuver. (*Right*) Post-fit range residuals produced from the EKF showing that after two measurements, the residual behavior is stable, thus suggesting that residuals and innovations covariance could be a first order approximation to indicate state stability, followed by the full covariance convergence time estimate.

It seems that for this orbital altitude, the uncertainty convergence is sensitive to observation consistency and station geometry. Assuming consistent measurements, priority tasking, and ideal station coverage, it also seems plausible that the uncertainty convergence time could be improved to near 10 minutes. While the 3σ uncertainty is a good method to confidently resolve an RSO's state, it may not be the only way to allow near real time estimation. For the same simulation, the residuals and innovations covariance can give clues to solution stability. After only two measurements, the range residual has stabilized and the 3σ innovations covariance has achieved a steady 20-meter value. Thus, it seems generally plausible to estimate Table 2 and 3 parameters within about 5 minutes of an active satellite maneuver using this technique and related assumptions. Studying residual behavior to indicate state stability should be used with caution as residuals alone do not guarantee an accurate orbit and thus should be later verified with the traditional state covariance. It makes sense to think of the RSO state stability study via residuals as a first order approximation that

allows for quicker estimation. The higher order, more accurate estimation could come later with the covariance convergence.

Once the RSO state is resolved post maneuver, back propagation to the maneuver end epoch and comparison to the nominal trajectory without the maneuver will reveal the delta-v magnitude and direction. Implementing this method and comparing to truth states provided by Optus for a N-S station keeping maneuver yielded a delta-v estimate within 0.51% of the true value. Maneuver type was estimated by comparing orbital elements pre- and post-maneuver as well as looking at the delta-v vector in the RIC frame. Using a ± 0.50 second uncertainty on the maneuver end epoch provided a delta-v magnitude estimate to within 7.84% (+0.50 sec) or 59.78% (-0.50 sec) of the true value, thus placing importance on maneuver detection epoch accuracy. The dynamic model used for the propagation of the Optus satellite included a 20x20 EGM-96 gravity model, luni-solar perturbations, exponential drag, and an area-averaged solar radiation pressure model. A complex Earth model using an FK5 precession, nutation, and polar motion correction was also implemented. The only assumptions made were that a ballistic coefficient and equivalent solar coefficient-area-mass combination were estimated via observations made on the object prior to observing a maneuver. The ballistic and solar values can be calculated the same way the JSpOC provides the estimated parameters for a secondary RSO in a conjunction data message (CDM). The duration of the maneuver was relatively short so the effects of drag and solar radiation pressure at GEO could be excluded and still achieve the same relative delta-v estimation accuracy.

Table 2. Estimation results of an Optus satellite maneuver in GEO compared to true values

Parameter	Estimation Accuracy	Notes
Delta-v magnitude	Within 0.51% of true value	-
Delta-v direction	Within 1.72 deg of true pointing vector	-
Maneuver type	SMA (a) lowered, Incl. (i) & Ecc. (e) increased	N-S station keeping

5. SPACECRAFT OPERATIONAL ASSESSMENT

With a known delta-v magnitude and direction, it should be possible to estimate spacecraft mass and thruster mass flow rate by using conservation of energy and momentum. The key to allowing this sort of analysis is the direct observation of event duration. Prior to applying high-rate photometric data as an event detection methodology, there were large errors in maneuver start and end time estimation due to the inability to directly observe the event. Applying the two principles between the now known start and end maneuver epochs allows for the study of the work performed and impulse imparted on the active satellite by the thruster event. Beginning with the basic form,

$$\bar{h} = \bar{r} \times \bar{v} \tag{1}$$

$$\varepsilon = \frac{1}{2}v^2 - \frac{\mu}{r} \tag{2}$$

and continuing to extend the energy and momentum equations to full three-dimensional space with the impulse and work terms included yields,

$$\begin{aligned} m_i \bar{r}_i \times \bar{v}_i + \int_{t_i}^{t_f} \bar{r}(t) \times (m_i - \dot{m}t)\left[\bar{a}_{thrust} + \bar{a}_{SRP} + \bar{a}_{drag} + \ldots\right] dt \\ + \int_{t_i}^{t_f} \bar{\tau}(t)\, dt + I_i \bar{\omega}_i + h_i = (m_i - \dot{m}\Delta t)\, \bar{r}_f \times \bar{v}_f + I_f \bar{\omega}_f + h_f \end{aligned} \tag{3}$$

where m_i, $\bar{r}_i$, and $\bar{v}_i$ are the initial mass, position, and velocity respectively with corresponding subscripts for the final values. The position as a function of time, $\bar{r}(t)$, is known based on the ability to fit a trajectory between the maneuver start and end states that are also known. Any non-conservative accelerations should be included within the brackets for the orbital impulse term. The attitude torque, $\bar{\tau}(t)$, initial and final moment of inertia, I_i and I_f, initial and final angular velocity, $\bar{\omega}_i$ and $\bar{\omega}_f$, and any momentum wheel terms, h_i or h_f, will be discussed later. Mass flow rate and maneuver duration are defined as $\dot{m}$ and Δt respectively. Continuing with the work-energy formulation,

$$\frac{1}{2}\, m_i \bar{v}_i^2 + \frac{1}{2}\bar{\omega}_i^T [I_i]\bar{\omega}_i - \, m_i [U_E(\bar{r}_i)] + \int_{t_i}^{t_f} \bar{F}(t) \cdot \bar{v}(t) dt + \int_{t_i}^{t_f} \bar{L}(t) \cdot \bar{\omega}(t) dt = \frac{1}{2}\, (m_i - \dot{m}\Delta t) \bar{v}_f^2 + \frac{1}{2}\bar{\omega}^T \left[I_f\right]\bar{\omega} - \, (m_i - \dot{m}\Delta t)\left[U_E\left(\bar{r}_f\right)\right] \tag{4}$$

where U_E is defined as the spherical harmonics formulation of gravitational potential energy as in [14]. Velocity as a function of time, $\bar{v}(t)$, is also known in the same way $\bar{r}(t)$ was derived. Any terms included in the rotational work integral, like $\bar{L}(t)$ and $\bar{\omega}(t)$, will be discussed in the next section.

$$U_E = \frac{\mu}{r}\left[1 + \sum_{l=2}^{\infty}\sum_{m=0}^{l}\left(\frac{R_E}{r}\right)^l P_{l,m}\left[\sin\left(\varphi_{gc}\right)\right]\left\{C_{l,m}\cos m\lambda + S_{l,m}\sin m\lambda\right\}\right] \tag{5}$$

Losses due to imperfect thrust vectoring, momentum wheel saturation, or the change in moment of inertia due to decreasing spacecraft mass are assumed to be negligible for a nadir-pointing, three-axis spin stabilized satellite. Thus, the rotational energy, work, torque, and momentum terms cancel out over the time span of the maneuver. Also, the only acceleration terms that need to be included in the work and impulse expressions are those relating to the propulsive event because the initial and final states were generated with the full force model described in earlier sections. It is also assumed that the acceleration due to thrust is an average value over the maneuver interval and thus does not account for any thrust profile effects. If more than one thruster were used, an n-multiple divisor would be needed to get individual thruster parameters. Using the standard rocket equation and definition of specific impulse yields an expression for the acceleration due to thrust as follows,

$$F_{thrust} = \, I_{sp} g_0 \dot{m} = \, m a_{thrust} \tag{6}$$

$$\frac{\Delta m}{m_i} = \, 1 \, - \, e^{-\Delta v / I_{sp} g_0} \tag{7}$$

$$\bar{a}_{thrust}(t) \, = \frac{-\Delta v \, \dot{m}}{(m_i - \dot{m}t) \, ln\left[1 - \frac{\dot{m}\Delta t}{m_i}\right]} \, \hat{a}(t)_{thrust} \tag{8}$$

where I_{sp} and g_0 are the specific impulse and sea level gravitational acceleration values. The change in mass is Δm, delta-v magnitude is Δv, and $\hat{a}$ is the time dependent thrust unit vector. The acceleration due to thrust term must be vectorized as the initial form of Eq. (6) is a scalar. It is also noted that the rocket equation formulation is idealized for impulsive maneuvers, when in reality the durations for many GEO station keeping maneuvers are non-impulsive. However, it is shown that the formulation still provides accurate results over the maneuver timespans discussed in this research but should be used with caution in the future. With a known delta-v vector and maneuver duration, one can numerically fit a fourth order polynomial to the acceleration values from burn start to end epochs. The polynomial vector itself could be used in Eq. (9) and Eq. (10) in place of the main analytical expression shown in Eq. (8), but we leave it mainly analytical to reduce any numerical errors associated with the empirical polynomial fit and to provide a formulation better prepared for future Monte Carlo analysis. The position and velocity as a function of time can similarly be fit with a fourth order polynomial after using the derived numerical acceleration function to propagate a trajectory between start and end epochs. The final form of our impulse-momentum equation is now as follows,

$$m_i \bar{r}_i \times \bar{v}_i + \int_{t_i}^{t_f} \bar{r}(t) \times \left[\frac{-\Delta v \, \dot{m}}{ln\left[1 - \frac{\dot{m}\Delta t}{m_i}\right]} \, \hat{a}(t)_{thrust}\right] dt = \, (m_i - \dot{m}\Delta t) \, \bar{r}_f \times \bar{v}_f \tag{9}$$

and for work-energy,

$$\frac{1}{2}\, m_i \bar{v}_i^2 - \, m_i[U_E(\bar{r}_i)] + \int_{t_i}^{t_f} \left[\frac{-\Delta v\, \dot{m}}{ln\left[1 - \frac{\dot{m}\Delta t}{m_i}\right]}\, \hat{a}(t)_{thrust} \right] \cdot \bar{v}(t)dt = \, (m_i - \dot{m}\Delta t) \left[\frac{1}{2}\, \bar{v}_f^2 - \, \left[U_E(\bar{r}_f)\right] \right] \quad (10)$$

At first glance, the system looks to consist of two equations and two unknowns. However, due to how Eq. (1) and (2) are formulated as specific energy and specific momentum values, the conversion from specific to mechanical energy and momentum sheds the linear independence with respect to the mass and mass flow rate terms. Thus, when attempting to solve for the two unknowns, the equations yields no solution. A first attempt around this is to run mass-mass flow rate pairs in a Monte Carlo fashion to see which pair yields the most balanced energy or momentum equation. However, the solution space for this method is not unique and thus produces ambiguous mass-mass flow rate pairs as shown in Fig. 4, normalized and purposely biased for proprietary reasons. It should also be noted that the solution is sensitive to the order used in the gravitational potential energy formulation. In this case, at least a 6x6 gravity field was needed at GEO to achieve the most accurate estimates.

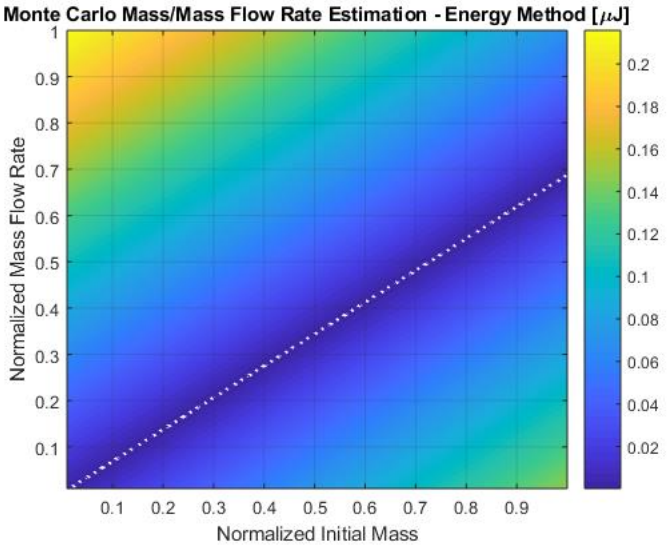

Simulation note: mass and mass flow rate pairs varying from +/- one order of magnitude about the true value were input into the work-energy equation, Eq. (10). The step size per pair was 1/100th of the maximum value. All values are normalized and purposely biased for proprietary reasons. The goal of this Monte Carlo analysis was to determine if one pair produced a unique global minimum that would balance the energy equation and thus be closest to the true values. As can be seen, the solution space is linear and produces ambiguous mass-mass flow rate pairs that balance the energy equation.

Fig. 4. Mass and mass flow rate pairs were run using Eq. (10) to determine if a solution could be found. The solution space is not unique, and many pairs produce the global minimum.

To summarize, it was proven that mass flow rate, fuel consumed, specific impulse, and exhaust velocity can be accurately estimated if given an a priori mass estimate. The a priori mass estimate is required due to the linear dependence of the mechanical angular momentum and energy formulations. Using the true Optus spacecraft mass yielded the estimates and error magnitudes shown in Table 3. Exhaust velocity is a secondary estimate that comes from getting specific impulse and mass flow rate. Explicit values for the thrust force as well as total impulse and change in energy due to the maneuver can also be calculated from the known parameters if desired.

Table 3. Estimation results for the Optus spacecraft operational parameters

Parameter	**Accuracy**	**Notes**
Mass flow rate ($\dot{m}$)	Within <2% of truth	-
Specific impulse (I_{sp})	Within <3% of truth	-
Fuel consumed (Δm)	Within <1% of truth	-
Exhaust velocity (v_e)	Agrees with generic values	True value not provided

The results demonstrate the importance of efforts in the Space Situational Awareness (SSA) community to estimate RSO mass and the resulting operational assessments that can be gained through estimates of the Table 3 parameters. One mass estimation method that seems promising uses astrometric and photometric data fusion [15]. Utilizing this method to get a good a priori mass estimate would resolve the pair ambiguity problem in Fig. 4.

One potential impact of estimating fuel consumption over time is the ability to monitor if an uncooperative satellite is saving enough fuel for a proper post-mission disposal or graveyard orbit. An estimate of specific impulse also helps characterize the operational capability of an active satellite. Of course, this research assumes the maneuvers happen at night and the start and end epochs of the propulsive event are directly observable via a ground based optical telescope. For satellites in LEO this could be a challenge, especially for longer, non-impulsive maneuvers. It seems plausible to employ these tactics to satellites in GEO based on a more stationary orbit. A satellite to satellite observation would likely make this method much more feasible as the relative distances and effects of the atmospheric would be lessened, thus increasing the signal to noise ratio and thruster event observability.

Assuming the Table 3 parameters are known in addition to the operational frequency and potentially a derived thrust profile, it's conceivable to compare these propulsion system values to known model specifications and thus constrain a specific class or even unique model to an observed event. Identifying a thruster model may help with other RSO identification parameters such as launch date or country of origin.

6. OBSERVATIONS

The initial goal of this research was to observe an active satellite thruster fire event in geosynchronous orbit (GEO). Satellite operators at Optus were kind enough to provide their maneuver schedule such that a precise orbital location and epoch were known for each observation. The optical telescope used was courtesy of the SERC 0.7-meter geotracker at the Mt. Stromlo Observatory in Australia. The high sampling rate detector is based on a Hamamatsu PMT sensor (H11901-20) that is highly sensitive over the entire visible spectrum. The photometric data is sampled at a rate of 50 kHz (up to 100 kHz), time stamped in UTC via GPS signal and stored in binary files. The detector is built on the Beaglebone Black PC board with the real time operation software written in C++.

So far, observations on the Optus constellation have not yielded a maneuver detection in the photometric, frequency, nor acoustic domains. The signal to noise ratio may simply not be good enough to detect any vibrational modes induced at GEO. It is likely that any activated modes did not have large enough relative displacements to be pulled from the noise floor or were simply damped by the satellite structural properties. With little atmosphere remaining at GEO, the chance to detect a plume or exhaust emission may be just as difficult. It's also possible the thrusters were oriented or masked by the satellite body in such a way relative to the telescope that it did not have a direct line of site to the exhaust vector. To continue the maneuver hunt, the team switched focus to LEO and MEO.

Over 20 hours of data on 29 unique active satellites including the Optus, GLONASS, and Iridium constellations as well as Ajisai, Cosmos 2527, and Sentinel 1a & 1b were collected by the SERC team from 2018-05-29 to 2018-08-16. The team rigorously quantified and removed any noise sources detected by the highly sensitive equipment. While no apparent propulsive events have been detected yet, some of the more interesting events and false positives are presented below to demonstrate the capability of the photoacoustic playback, event detection methodology, and high sampling rate detector performance. It should be noted that the LEO and MEO observations did not include collaboration with any satellite operators to confirm whether an arc would have a maneuver within the collection period prior to observing. However, if there were an unexplained anomaly in the data, operators at Iridium and Optus were kind enough to provide any correlation to on-board events, if any such correlation existed. Secondary measurements from LeoLabs also helped determine whether unexplained signals could be correlated to any RSO unmodeled dynamic events.

Iridium 14 Flare

Data collected on Iridium 14 revealed a classic flare, or abrupt peak in visual magnitude, due to favorable observation geometry and the relative attitude progression throughout its orbit. The flare included two auxiliary peaks on either side of the main peak. It is likely the auxiliary peaks were caused by door-sized antennas offset by 40 degrees from the panel antenna that is known to cause the main flare in light intensity.

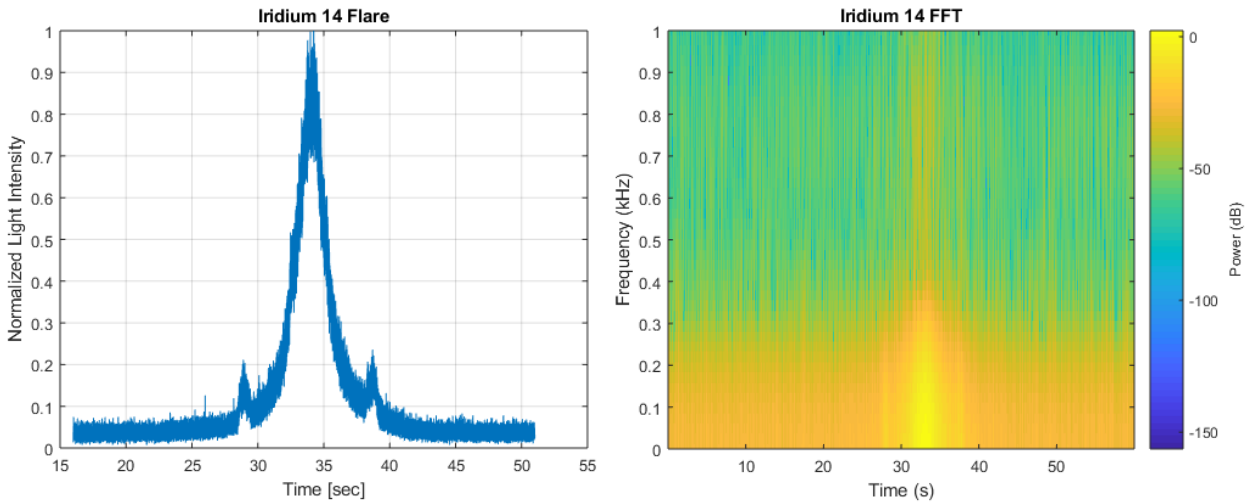

Fig. 5. (*Left*) A plot of normalized light intensity over time showing the main flare and auxiliary peaks likely due to the 40 deg offset panel antennas. Depending on flare magnitude, clipped peak light intensity values may be possible. (*Right*) Frequency content of the Iridium 14 flare data shown via FFT and displayed as a spectrogram.

The photoacoustic playback of the flare allows for detection of the main intensity rise and fall as well as the auxiliary peaks. As this is a common satellite event that is easily detected in the photometric domain, the audio playback doesn't reveal any unique insights besides it being a demonstration of the acoustic domain conversion and an interesting listen. The general aural perception could be described as, "Increasing, then decreasing white noise, with two abrupt transients on the downslope and upslope." One could imagine if a propulsive event occurred during or near a flare that the potential thruster-induced modulation of the flat panel antennas and corresponding harmonics would be easily detectable due to the high apparent visual magnitude over this timespan.

Ajisai Tumble Chirp

The Experimental Geodetic Payload (EGP) satellite Ajisai was a great calibration object for the photodiode system. Ajisai has a known spin rate of 1.25 Hz which can be seen in the Fig. 6.

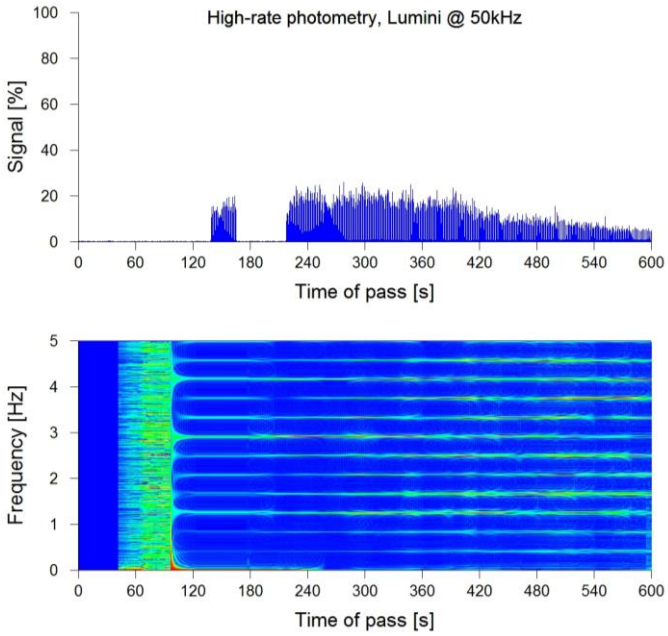

Fig. 6. (*Top*) Ajisai pass light intensity peaks over time. (*Bottom*) Frequency spectrum obtained with the open source FFTW tool. The parallel lines indicate the harmonics of the satellite spin frequency signal of 0.4167 Hz.

The photoacoustic playback of Ajisai's signal could be described as a "partially muted tumble chirp" that peaks at the indicated rate of 1.25 Hz (3x the base frequency described in Fig. 6). Like the flare, this is a relatively well-known phenomenon that is studied in the photometric domain. Like the Voyager 1 example, the Ajisai tumble chirp audio playback comes from generating an acoustic signal from an event that is inherently non-acoustic to support analysis and event detection. The acoustic domain conclusions for this observation would be a confirmation of typical behavior and an interesting pulsation to listen to! Collecting photoacoustic data on a decommissioned satellite that has a spin rate like Ajisai could yield unique signatures. One could imagine the spin induced "crackling" sound the multi-layer thermal insulation blankets (MLI) could produce on the decommissioned satellite would be unique compared to the clean tumble chirp generated by the non-flexible mirrors mounted on the exterior surface of Ajisai.

SLR Ticking

In many of the collected data arcs, a 10 Hz and sometimes a 60 Hz signal would show up briefly and then disappear with no apparent correlation to satellite events. The signal itself sounded like a "reverberating tick" that was easily identifiable whenever it appeared. Eventually, it was discovered that the nearby satellite laser ranging (SLR) equipment operation correlated exactly with the signal epochs. While the SLR operated at 60 Hz, the photometric system became blind during the laser pulses approximately every 100 ms due to what is likely a time domain aliasing effect. Thus, the 10 Hz signal can be acquired in the FFT. One example of the 60 Hz detection is shown in Fig. 7.

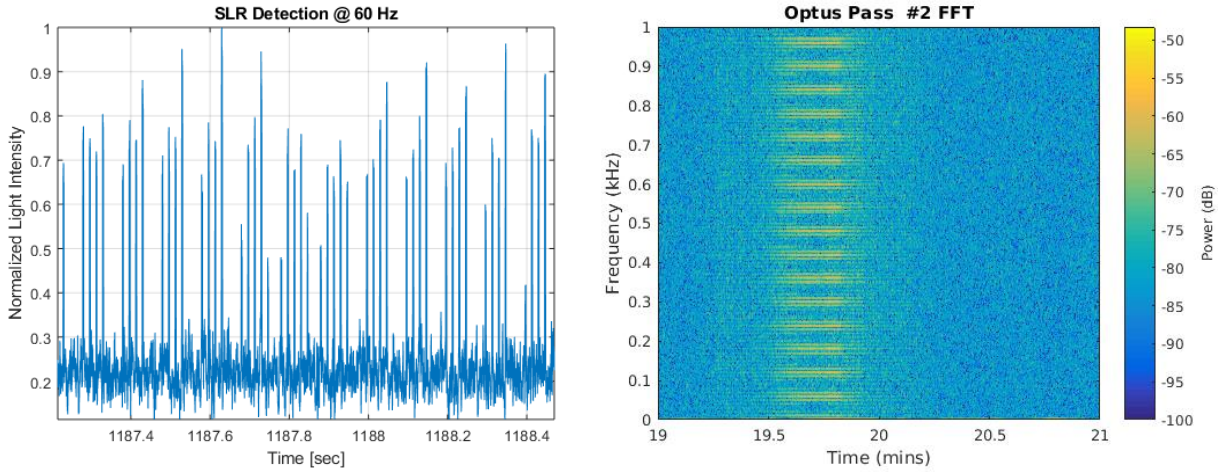

Fig. 7. (*Left*) Light intensity plot showing the peaks due to the nearby SLR operation. (*Right*) The 60 Hz laser pulse fundamental frequency and harmonics detected when the SLR field of view (FOV) crossed the geotracker FOV.

Telescope Tracking Stability

The most exciting false positive signal detected was caused by a tracking stability problem as the telescope operated at a high speed while the tracked satellite was at a high elevation angle above the local horizon. It even looked as if there were some sort of pre-ignition sequence event detected due to a minor peak approximately 6.5 seconds before the main light intensity increase. The signal in Fig. 8 looks quite like the abrupt peak that would be expected for a thruster plume detection, as well as the exponential "thrust profile-like" tail off.

Australian Power Grid

Another mystery signal was explained by the Australian power grid that operates at 50 Hz. A commonly observed phenomenon is the flickering of exterior lights in close proximity to the observatory at two times the grid frequency as shown in Fig. 8. The lights are motion sensor activated and thus can show up sporadically in the data.

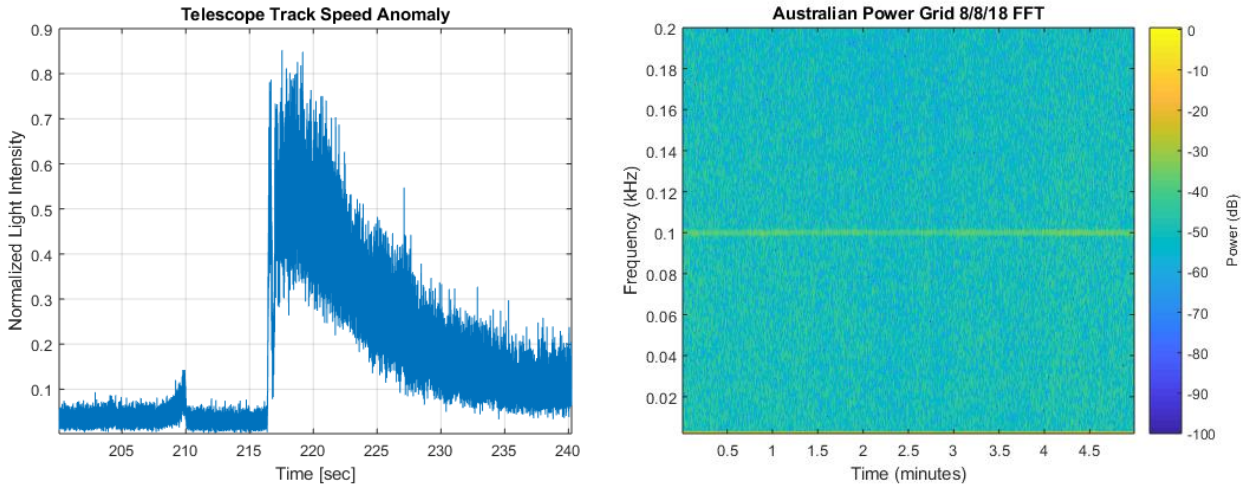

Fig. 8. (*Left*) Light intensity plot showing the abrupt peak caused by the telescope track stability problem described above. (*Right*) FFT that detected the Australian power grid lights flickering at 2x the 50 Hz grid frequency.

Short Burst Transients

A still unexplained signal that showed up at least twice in two different satellite collections could be described as a short burst transient. Each time the profile appeared in the data there were two distinguishable peaks as seen in Fig. 9. There were many other cases where a star passed the FOV which caused a gradual rise and fall in light intensity. The transients seem much too quick to be explained by a star passing. Acoustic playback of the potential events sounds somewhat noisy but does have a detectable "dual burst" characteristic to it. It is possible these are some sort of measurement system aberration. The frequency content is quite rich in the sub-20 Hz range. More investigation will be needed to identify what may have caused these transients.

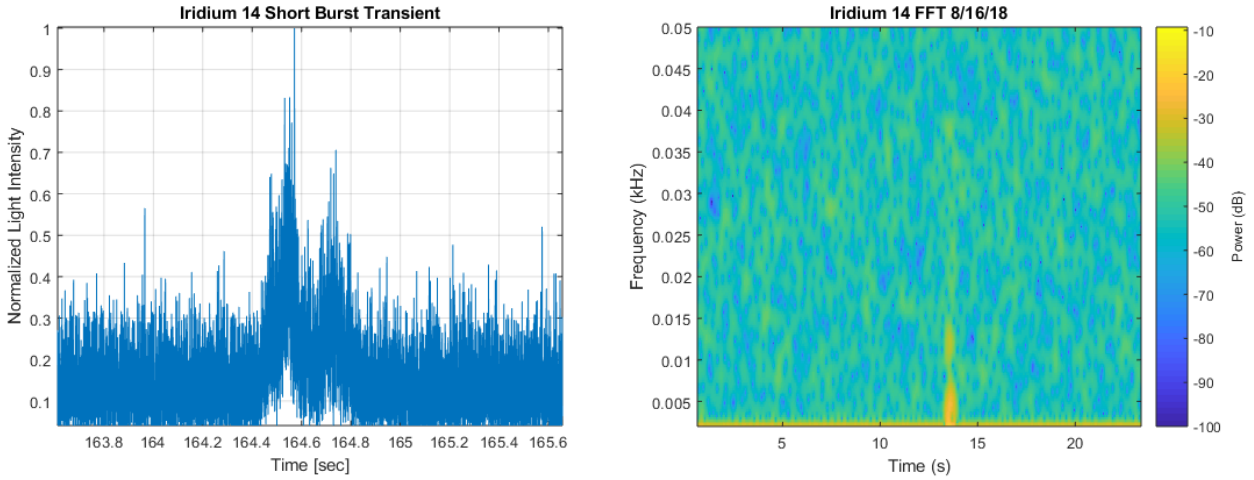

Fig. 9. (*Left*) Light intensity plot of the uncorrelated short "burst" transient profile seen in multiple data collections. A unique characteristic of this profile is that it always seems to have a double peak and is less than one second in duration. (*Right*) FFT of the same event. The most powerful frequency components are sub-20 Hz.

7. FUTURE WORK

While this research had a heavy focus in maneuver detection and estimation, photoacoustic sensing also has great potential to discover casual relationships in any RSO observed phenomena that could lead to their characterization, classification, and unique identification. Categorizing RSOs by their biometric modalities would be a logical next step in exploiting remote photoacoustic signatures. It is the hope of this research that as enough data is collected, patterns start to emerge based on RSO type, regime, and other characteristics. To support maneuver detection, implementing

a more advanced method to pull signals from the noise floor such as cross-correlation could improve the minimum detectable displacement threshold. There may be further improvements in the optical domain realized by reducing the telescope FOV. Other methods specific to detecting a thruster plume as opposed to the modulated surface could also be investigated. It would also be good to extend the RSO state resolution time study post-maneuver to GEO to determine how observability and measurement consistency affect the uncertainty convergence in a different orbital regime. The loss of linear independence when formulating mechanical energy and angular momentum disallowed this method to be a standalone way to estimate mass, mass flow rate, and any other derived parameters. If there were some way to inject linear independence back into the system of two equations or to resolve the pair ambiguity, it would enable standalone mass estimation. Finally, the observation goal remains to experimentally detect an active satellite propulsion system activation event. Further collaboration with willing satellite operators will be a key component to capturing a maneuver.

8. CONCLUSIONS

This work proposed a new method to support characterization of resident space objects by exploiting remote photoacoustic signatures. Interpreting high-rate photometric data as a photoacoustic signal yields insight into RSO behavior and likely provides unique signature interpretations that can be used as biometric modalities to identify active satellites and on-board component level events such as a thruster activation. With a maneuver start and end epoch derived from high-rate photometric data, it was shown that a first order approximation of the burn duration, forcing frequency, delta-v magnitude, direction, and maneuver type could be accurately estimated within five minutes of thruster off-time. This sort of near real time estimation scheme increases general SSA capabilities and supports operational risk reduction by greatly shrinking the maneuver detection lag. It was also shown that with an a priori estimate of spacecraft mass, the thruster mass flow rate, specific impulse, exhaust velocity, and fuel consumed by a maneuver could be accurately estimated via impulse-momentum and work-energy methods. This list of satellite operational parameters helps characterize its mission, capability, and may even lead to the ability to identify unique thruster models which could support country of origin determination or similar identity-related inquiries. The ability to audit fuel consumption supports efforts to monitor uncooperative satellite behavior for proper post-mission disposal orbits and mission lifetime estimates.

The output of this research provided further motivation to experimentally detect an active satellite thruster fire event. The resulting analysis that can be attained from such an event shows great promise in uniquely characterizing RSOs and assessing operational capability.

9. ACKNOWLEDGEMENTS

The authors would like to thank Dan Slater and Rex Ridenoure for the initial seed idea that pointed us towards high-rate photometry and the light to sound conversion in the first place. Also, a bravo and thank you is deserved of our colleagues at SERC and EOS Space Systems, specifically Dr. James Bennett, Dr. James Webb, and Dr. Daniel Kucharski, for the data collection and high-rate sampling detector set up. None of the experimental observations would have been possible without this collaboration. The team would also like to acknowledge the collaborative efforts of Andrew Edwards, Tim Lilley, and Anthony Belo of Optus. We would also like to thank Dr. Tamara Payne for valuable discussions regarding light curve simulations and Dr. Jayant Sirohi for insight on potential box-wing vibration modes. The authors would like to thank Dr. Preston Wilson for valuable discussions on acoustics. Also, the collaborative sharing efforts of the Iridium operators were much appreciated – we hope to continue this in the future. We would also like to thank LeoLabs for their maneuver detection support and helpful data analysis. Finally, we'd like to thank Vishnuu Mallik for helpful references on light curve, range, and range-rate measurement simulations.

10. REFERENCES

[1] Slater, D., Ridenoure, R., Klumpar, D., Carrico, J., and Jah, M. "Light to Sound: The Remote Acoustic Sensing Satellite (RASSat)." *30th Annual AIAA/USU Conference on Small Satellites*, Logan, Utah, 2016.

[2] Bell, A.G., "On the Production and Reproduction of Sound by Light." *American Journal of Sciences*, Third Series, vol. XX, no. 118, Oct. 1880, pp. 305-324.

[3] Davis, A., et. al., "The Visual Microphone: Passive Recovery of Sound from Video," *ACM Transactions on Graphics*, vol. 33, Issue 4, Article No. 79.

[4] Dennis, J., Yu, Q., Tang, H., Tran, H., and Li, H. "Temporal coding of local spectrogram features for robust sound recognition," *Acoustics, Speech and Signal Processing (ICASSP), 2013 IEEE International Conference*, 26-31 May 2013 DOI: 10.1109/ICASSP.2013.6637759.

[5] The Agency for Science, Technology and Research (A*STAR). "Audio processing: Computers following the brain's lead." ScienceDaily. ScienceDaily, 6 November 2013. Retrieved from <www.sciencedaily.com/releases/2013/11/131106084430.htm>.

[6] Gurnett, D.A., Kurth, W.S., Burlaga, L.F., and Ness, N.F. "In Situ Observations of Interstellar Plasma with Voyager 1," *Science*, vol 341, pp. 1489-1492. 12 September 2013, DOI: 10.1126/science.1241681.

[7] Jain, A., Ross, A., and Prabhakar, S. "An Introduction to Biometric Recognition," *IEEE Transactions on Circuits and Systems for Video Technology*, vol 14, No. 1, January 2004.

[8] Adeoye, O. "A Survey of Emerging Biometric Technologies," *International Journal of Computer Applications*, vol. 9, No. 10, November 2010.

[9] Kelecy, T., and Jah, M., "Detection and orbit determination of a satellite executing low thrust maneuvers." *Acta Astronaut*, vol. 66, 2010, pp.798–809.

[10] Aaron, B.S., "Geosynchronous satellite maneuver detection and orbit recovery using ground based optical tracking." Masters Thesis, Massachusetts Institute of Technology, 2006.

[11] Wetterer, C.J., and Jah, M. "Attitude Estimation from Light Curves," *Journal of Guidance, Control, and Dynamics*, vol. 32, No. 5, 2009, pp. 1648-1651.

[12] Dorival, O., Rouch, P., et. al. "Vibration Tests on a Satellite-like Structure." Département de Génie Mécanique, ENA Cachan. Retrieved from <https://www.youtube.com/watch?v=dUewH84jNw8>.

[13] Halverson, R. "Final Boost Stage of GSSAP and ANGELS satellites." Dakotalapse. 28 July 2014. Retrieved from <http://dakotalapse.com/2015/01/final-boost-stage-4k-uhd/>.

[14] Vallado, David A. *Fundamentals of Astrodynamics and Applications*. Microcosm Press, 2013, Print. Fourth Edition.

[15] Mallik, V., Jah, M.K. Reconciling space object observed and solar pressure albedo-areas via astrometric and photometric data fusion. Adv. Space Res. (2018), https://doi.org/10.1016/j.asr.2018.08.005